PHYSICAL REVIEW B VOLUME 27, NUMBER 2 15 JANUARY 1983

Guided-wave polaritons in thin films of the layered compound GaSe

Y. Sasaki* and S. Ushioda
Department of Physics, University of California, Irvine, California 92717

(Received 3 May 1982)

Guided-wave polaritons (GWP) in thin uniaxial crystals of ϵ-GaSe (D_{3h}^1) have been studied by means of near-forward Raman scattering. GaSe was chosen as the convenient sample system for this study because it forms a layered compound crystal that can be cleaved into very thin films with varied thickness and smooth surfaces. The samples were prepared from bulk ϵ-GaSe by cleavage with the crystallographic c axis normal to the plane of the film. The film thickness (d) ranged between 2.7 and 6.5 μm. In a uniaxial crystal, infrared-active phonons propagating along a general direction split into three modes: two branches of extraordinary waves (EX_1 and EX_2 branches) and one branch of ordinary waves (OR branch). The ordinary waves are pure TO phonons which form volume polaritons and GWP. The extraordinary waves are admixtures of TO and LO phonons; thus these waves also form volume polaritons and give rise to GWP in a film geometry. In this work both the mode dispersion and the Raman scattering intensity of GWP and surface polaritons were measured for the infrared- and Raman-active E' mode appearing between ~ 180 and ~ 300 cm^{-1}. The dispersion of the observed surface modes, including the film-thickness dependence, agrees with theory after appropriate adjustments are made for the dielectric function of ϵ-GaSe in the far infrared. The Raman scattering intensity can be fitted with the use of a phenomenological theory based on the bulk Raman tensor. The agreement between the measured and the calculated spectra is very good for thick samples ($d \geq 5$ μm). The deviation from the calculated spectra in the thinnest sample (2.7 μm) can be understood when one takes into account the damping of GWP upon reflections at the surface.

I. INTRODUCTION

The existence of a surface in a semi-infinite crystal gives rise to surface polaritons (SP) which propagate along the surface with a real wave vector $\vec{k}_{||}$ and whose amplitude decays exponentially away from the surface.[1,2] Corresponding to the amplitude decay away from the surface, the wave-vector component of SP normal to the surface ($\vec{k}_\perp$) is purely imaginary. When there are two parallel surfaces, i.e., in a film geometry, there are two kinds of surface modes depending on whether $\vec{k}_\perp$ inside the film is real or imaginary. If $\vec{k}_\perp$ is imaginary, the mode amplitude decays into the film and away from the film exponentially. There are two modes of this kind corresponding to SP's arising from the two surfaces (the upper-mode and lower mode, UM-SP and LM-SP, respectively). These modes are degenerate if the film thickness d is much greater than $2\pi/k_\perp$, but split into two distinct frequencies for $d \lesssim 2\pi/k_\perp$. We call these modes SP; they are called double-interface modes in Ref. 2. On the other hand, if $\vec{k}_\perp$ is real, the mode amplitude decays away from the film but oscillates inside; these modes are called guided-wave polaritons (GWP) because their amplitude pattern is similar to that of waveguide modes. Because of the finite thickness of the film, $\vec{k}_\perp$ is quantized to be near multiples of π/d, and the ampltiude variation along the thickness of the film has a standing-wave pattern.[2,3] In the visible and near-infrared frequency regime, GWP's are used in integrated optics.[4] The SP's in the far infrared that arise from the optical phonons have been investigated by the attenuated-total-reflection (ATR) method[1] and by Raman scattering.[2] The GWP's formed by optical-phonon polaritons were observed by Raman scattering in cubic GaP by Valdez, Mattei, and Ushioda (VMU).[5]

The main purposes of this paper are threefold. The first purpose is to extend the work of VMU to GWP's in an anisotropic crystal where more complex mode dispersions are expected. The second purpose is to investigate the thickness dependence of the GWP and SP dispersion relations. This kind of study could not be made by VMU because of the difficulty of preparing very thin samples (10—60 μm) of GaP by polishing. GaSe is an ideal crystal because it can be easily cleaved into very thin films of several micrometer thickness. The third purpose is to assess the effect of surface roughness on the SP and GWP dispersion relations and the Raman scattering intensities by using samples with atomically smooth surfaces. VMU found that the measured Raman scattering intensity varied depending on surface conditions and also that the intensity predicted by theory[6] did not agree with the experimental results. In the case of the layered compound ϵ-GaSe, the surfaces of cleaved films are smooth on the atomic scale. Adjacent layers are held by the van der Waals force; hence, the cleaved surfaces do not have any dangling bond and consist of wide terraces of atomically smooth planes. In this paper we attempt to compare theory to experimental results on SP and GWP in the absence of surface roughness which could not be avoided on GaP surfaces.

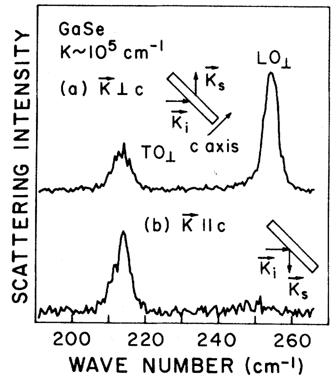

FIG. 2. Raman spectra of ϵ-GaSe: TO and LO phonons for large wave vectors propagating (a) normal to the c axis and (b) parallel to the c axis. Arrows in the insets indicate the wave vectors of the incident and the scattered light. The sample thickness is 6.5 μm.

We have chosen ϵ-GaSe among the many layered compounds, because its relevant properties in the far infrared are reasonably well established.[7–10] The ϵ-GaSe crystal has the D_{3h}^1 space-group symmetry with 8 atoms per unit cell. The Raman-active modes of this crystal have symmetries A_1', E', and E''. The backscattering spectrum of these bulk phonons are shown in Fig. 1 for reference purposes. Among these modes only the E' modes are simultaneously Raman and ir active with the polarization vector in the basal plane. The corresponding mode with the polarization vector along the c axis has the A_2'' symmetry, which is ir active but Raman inactive. Thus when the $\vec{k}$ vector is in the basal plane ($\vec{k}\perp c$), the E' modes split into the $\mathrm{TO}_\perp$ and $\mathrm{LO}_\perp$ modes both of which are Raman active. When the $\vec{k}$ vector is parallel to the c axis ($\vec{k}\,||\,c$), the doubly degenerate $\mathrm{TO}_\perp$ modes are Raman active, but the corresponding $\mathrm{LO}_{||}$ mode (A_2'' mode with the polarization along the c axis) is Raman inactive. This situation is experimentally observed as illustrated in Fig. 2. Note that for $\vec{k}\,||\,c$ no LO peak is observed, and also that the $\mathrm{TO}_\perp$ intensity for $\vec{k}\,||\,c$ is twice as strong as for $\vec{k}\perp c$, corresponding to the double degeneracy of the $\mathrm{TO}_\perp$ mode for this configuration. When the $\vec{k}$ vector makes an angle θ_p ($\theta_p \neq 0, \pi/2$) with respect to the c axis, one of the modes is a pure TO mode [ordinary wave (OR)] and two of the modes (EX_1 and EX_2 extraordinary wave modes) have a mixed character of the TO and LO phonons. The relationship between the propagation angle and the mode frequency is depicted in Fig. 3 for ϵ-GaSe. The small circles indicate that the modes corresponding to these points are Raman inactive. Figure 3 also shows the plot of $\epsilon_{||}(\omega)$ and $\epsilon_\perp(\omega)$ for ϵ-GaSe. The high-frequency extraordinary wave (EX_2 mode) is a pure $\mathrm{LO}_{||}$ mode when $\theta_p = 0$ and $\mathrm{LO}_\perp$ mode when $\theta_p = \pi/2$, but contains some transverse component for general propagation directions. Thus this mode (EX_2) as well as the two other modes (EX_1 and OR) forms polaritons and GWP, showing splitting according to the values of $\vec{k}_\perp$ and dispersion with $\vec{k}_{||}$.

ϵ-GaSe turns out to be a very convenient system to work with in other respects as well. It is semi-

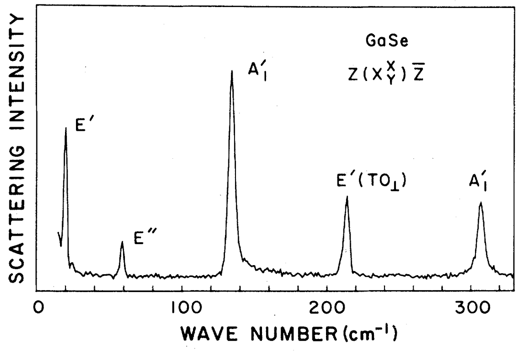

FIG. 1. Raman spectrum of ϵ-GaSe in a backscattering configuration.

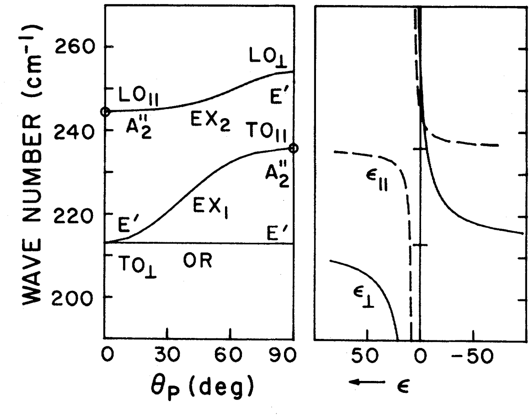

FIG. 3. Directional dispersion of LO and TO phonons and dielectric constants of ϵ-GaSe.

transparent in the visible spectrum, so that we can measure Raman scattering in a near-forward direction from a thin film. The fact that it absorbs light in the blue and green range means that we can expect Raman-intensity enhancement from near-resonant conditions. This is an important consideration when one works with the scattering path lengths on the order of several micrometers. The presence of nonpolar modes as shown in Fig. 1 allows us to calibrate Raman intensities from spectrum to spectrum taken under different conditions. We make use of this advantage in comparing the observed Raman intensities of SP and GWP with theoretical predictions.

In the following section we present a theory of SP and GWP in an anisotropic film (Sec. II A). Section II B deals with a phenomenological theory of Raman scattering intensities of SP and GWP. In Sec. III we present the experimental results, and Sec. IV is devoted to the discussion of the results. Section V contains concluding remarks.

II. THEORY

A. Dispersion relations

We consider electromagnetic waves that propagate parallel to the surface (x direction) in a free-standing uniaxial film of thickness $d \equiv 2a$ with the c axis normal to the surface. This geometry is illustrated in Fig. 4; media 1 and 3 have a frequency-independent dielectric constant $\epsilon_1 > 0$, and the uniaxial film (medium 2) has frequency-dependent dielectric constants $\epsilon_{2\perp}(\omega)$ and $\epsilon_{2\|}(\omega)$ for polarizations perpendicular and parallel, respectively, to the c axis. In the optical-phonon frequency region, $\epsilon_{2\|,\perp}(\omega)$ is given by

$$\epsilon_{2\|,\perp}(\omega)=\epsilon_{\infty\|,\perp}+\frac{(\epsilon_{0\|,\perp}-\epsilon_{\infty\|,\perp})\omega^2_{\mathrm{TO}_{\|,\perp}}}{\omega^2_{\mathrm{TO}_{\|,\perp}}-\omega^2}\,, \qquad (1)$$

where $\epsilon_{\infty\|,\perp}$ and $\epsilon_{0\|,\perp}$ are the optical and static dielectric constants, respectively; $\omega^2_{\mathrm{TO}_{\|,\perp}}$ is the TO-phonon frequency with the polarization vector either parallel ($\|$) or perpendicular ($\perp$) to the c axis. In Eq. (1) we neglect the damping of optical phonons; consequently, mode-damping effects are not explicitly included in the equations that follow. However, we will include small damping when we calculate the theoretical Raman spectra later.

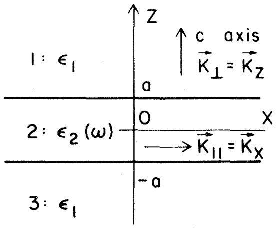

FIG. 4. Film geometry and coordinate system. Media 1 and 3 are air in the present experiment.

The λ Cartesian component of the electric field amplitude of the electromagnetic waves in the three regions of Fig. 4 can be written as

$$E_\lambda^{(1)}(\vec{x},t)=A_\lambda e^{i(k_\| x-\omega t)-\alpha z}\,, \qquad (2)$$

$$E_\lambda^{(2)}(\vec{x},t)=B_\lambda(e^{ik_\perp z}\pm e^{-ik_\perp z})e^{i(k_\| x-\omega t)}\,, \qquad (3)$$

$$E_\lambda^{(3)}(\vec{x},t)=C_\lambda e^{i(k_\| x-\omega t)+\alpha z}\,. \qquad (4)$$

Here $\alpha \equiv (k_\|^2-\epsilon_1\omega^2/c^2)^{1/2}$ is the real decay constant outside the film, and $k_\|$ and $k_\perp$ are the wave vectors inside the film for x and z directions, respectively. A_λ, B_λ, and C_λ are the amplitude constants for the three regions. When we substitute the above assumed forms of the waves into Maxwell equations with appropriate boundary conditions at $z=\pm a$, dispersion relations and eigenvectors for the normal modes of the geometry with different polarizations are obtained.

When $k_\perp$ is real the extraordinary optical-phonon branches (EX_1 and EX_2) give rise to transverse magnetic (TM) polarized GWP's with the implicit dispersion relations

$$\epsilon_\perp/\epsilon_1=(k_\perp/\alpha)\tan(k_\perp a) \qquad (5)$$

and

$$\epsilon_\perp/\epsilon_1=-(k_\perp/\alpha)\cot(k_\perp a)\,, \qquad (6)$$

where

$$k_\perp=[\epsilon_\perp(\omega^2/c^2-k_\|^2/\epsilon_\|)]^{1/2}\,. \qquad (7)$$

Here $\epsilon_\perp$ and $\epsilon_\|$ are shorthand notations for $\epsilon_{2\perp}(\omega)$ and $\epsilon_{2\|}(\omega)$ of Eq. (1). The solutions represented by Eqs. (5) and (6) are shown in Fig. 5 denoted by TM_1, TM_2, and TM_u. The branches TM_1 and TM_2 arise from the extraordinary phonon branches EX_1 and EX_2, respectively, and TM_u is the upper branch of TM which is mostly transversely polarized.

The ordinary optical-phonon branch (OR in Fig. 3) gives rise to transverse electric (TE) polarized GWP's whose dispersion is given by

$$1=(k_\perp/\alpha)\tan(k_\perp a) \qquad (8)$$

and

$$-1=(k_\perp/\alpha)\cot(k_\perp a)\,, \qquad (9)$$

where

$$k_\perp=(\epsilon_\perp\omega^2/c^2-k_\|^2)^{1/2}\,. \qquad (10)$$

The solutions given by Eqs. (8) and (9) are denoted by TE and TE_u in Fig. 5. We note that Eqs. (5), (6), (8), and (9) determine discrete allowed values of $k_\perp$ which in turn give the dispersion relations (ω vs $k_\parallel$) through Eqs. (7) and (10). The above four equations have a common asymptotic solution for large $k_\perp$ given by

$$k_\perp = m\pi/2a \ , \tag{11}$$

where m is a positive integer mode number for GWP's. For GWP's the electric field inside the film given by Eq. (3) can be rewritten as

$$E_\lambda^{(2)}(\vec{x},t)=2B_\lambda \begin{Bmatrix}\cos(k_\perp z)\\ i\sin(k_\perp z)\end{Bmatrix} e^{i(k_\parallel x-\omega t)} \ , \tag{12}$$

since $k_\perp$ is real. This expression shows that the field amplitude of GWP has a standing wave pattern across the thickness of the film and propagates sinusoidally along the surface plane. The integer m in Eq. (11) corresponds to the number of nodes of the standing wave. There is an alternative way of looking at GWP from the viewpoint of ray optics.[4] GWP can be interpreted as a wave that propagates in the film in a zigzag manner as illustrated in Fig. 6. The wave is totally reflected at the surface and propagates with the real wave vector given by $k_\parallel \hat{x} + k_\perp \hat{z}$, where $\hat{x}$ and $\hat{z}$ are the unit vectors along the x and z axis, respectively. The propagation angle θ_p has discrete values for a given value of $k_\parallel$ as $k_\perp$ is quantized. The increment between the allowed values of $k_\perp$ is roughly given by π/d. In the thick-film limit $k_\perp$ forms a quasicontinuum as in the case of an infinite three-dimensional crystal. When the mean free path of the modes is shorter than the film thickness, $k_\perp$ is not quantized, and one should observe a continuum of GWP's.

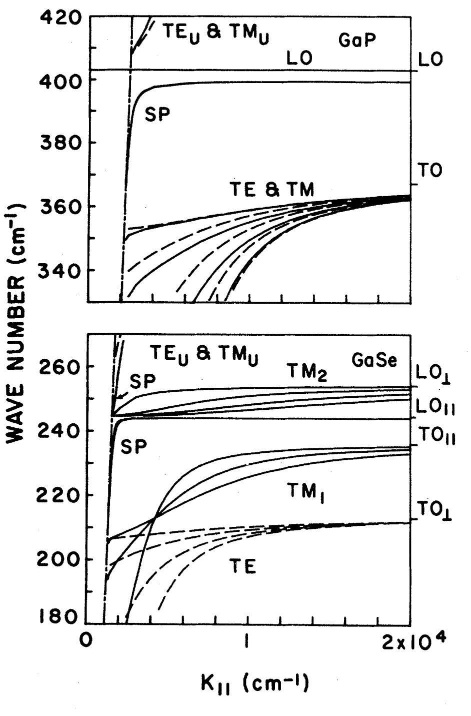

FIG. 5. Dispersion curves of GWP and SP in GaP and ϵ-GaSe. The film thickness is 10 μm. The dashed lines show TE modes and the solid lines show TM modes. The dot-dashed straight lines indicate the light line in vacuum.

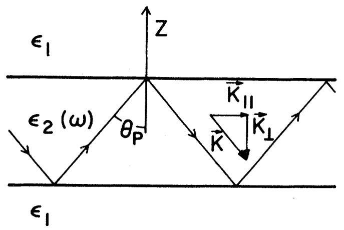

FIG. 6. Zigzag propagation model for GWP.

When $k_\perp$ is imaginary, the Maxwell equations with boundary conditions give the implicit dispersion relations for SP:

$$\epsilon_\perp/\epsilon_1 = -(\beta/\alpha)\tanh(\beta a) \tag{13}$$

and

$$\epsilon_\perp/\epsilon_1 = -(\beta/\alpha)\coth(\beta a) \ , \tag{14}$$

where $i\beta \equiv k_\perp$ is given by Eq. (7). Equations (13) and (14) correspond to the upper mode (UM) and the lower mode (LM) of SP's. In this case there is only one solution each for $k_\perp$ from Eqs. (13) and (14), and consequently there are only two branches, UM-SP and LM-SP, arising from these two equations. For the parameters of ϵ-GaSe used in Fig. 5 these branches are almost degenerate. For SP's the electric field inside the film given by Eq. (3) can be rewritten as

$$E_\lambda^{(2)}(\vec{x},t)=2B_\lambda \begin{Bmatrix}\cosh(\beta z)\\ \sinh(\beta z)\end{Bmatrix} e^{i(k_\parallel x-\omega t)} \ . \tag{15}$$

In Fig. 5 we show the dispersion curves of SP and GWP in the cubic crystal GaP for comparison purposes. The GaP sample thickness is assumed to be 10 μm; for this thickness the UM-SP and LM-SP are almost degenerate. The same is true for a 10-μm-thick sample of GaSe. Thus in both cases only one curve can be seen for SP. In GaP both TM GWP and TE GWP appear in the same frequency region, because the directions normal and parallel to the surface are equivalent. However, in the anisotropic GaSe film with the c axis normal to the film, TM GWP and TE GWP are split by the anisotropy. The origins of different branches of GWP can be understood clearly if one compares Fig. 5 with Fig. 3 where the mode frequencies are shown for large values of $\vec{k}$ in an infinite crystal of ϵ-GaSe. The θ_p dependence of the mode frequencies were calculated from the well-known equation for a uniaxial crystal[11]:

$$\omega^2/c^2k^2=\epsilon^{-1}(\omega)$$
$$=\frac{\epsilon_\perp(\omega)\sin^2\theta_p+\epsilon_{||}(\omega)\cos^2\theta_p}{\epsilon_\perp(\omega)\epsilon_{||}(\omega)}\,, \tag{16}$$

in the limit of $k\rightarrow\infty$. Hoff, Irwin, and Lieth[12] have shown that Eq. (16) fits the experimental directional dispersion of LO and TO phonons of γ-polytype GaSe at $\theta_p=0°$, 45°, and 90°. We note that the oscillator strength for $\vec{E}\perp c$ is much greater than that for $\vec{E}||c$ in ϵ-GaSe. Thus the splitting between $\omega_{\mathrm{TO}_\perp}$ and $\omega_{\mathrm{LO}_\perp}$ is much greater than the splitting between $\omega_{\mathrm{TO}_{||}}$ and $\omega_{\mathrm{LO}_{||}}$, both of which fall between $\omega_{\mathrm{TO}_\perp}$ and $\omega_{\mathrm{LO}_\perp}$.

For clarity we show only a few lowest branches of GWP of each group in Fig. 5. In the limit of $k_{||}\rightarrow\infty$, the asymptotic limiting frequencies of the TM$_1$-, TM$_2$-, and TE-GWP approach $\omega_{\mathrm{TO}_{||}}$, $\omega_{\mathrm{LO}_\perp}$, and $\omega_{\mathrm{TO}_\perp}$, respectively. In the limit of small $k_{||}$, TM$_2$ GWP's converge to $\omega_{\mathrm{LO}_{||}}$, while TM$_1$-GWP branches cross each other at $\omega_{\mathrm{TO}_\perp}$ and then approach the light line. The behavior of TE GWP is identical to that of TE GWP in an isotropic crystal, approaching the light line for $k_{||}\rightarrow 0$.

In anisotropic dielectrics, new SP branches appear in addition to the branches observed in isotropic materials. Such additional SP branches were observed in quartz by the ATR method.[13] In ϵ-GaSe an extra branch of SP appears between $\omega_{\mathrm{LO}_{||}}$ and $\omega_{\mathrm{LO}_\perp}$ near the vacuum-light line. The short segment is indicated by an arrow in Fig. 5.

B. Raman scattering intensity

The Raman spectra of GWP's in an isotropic crystal (GaP) have been calculated by Subbaswamy and Mills[6] using a Green's function approach. Here we use a simpler approach to calculate the Raman scattering intensities of SP and GWP's in a uniaxial crystal. First, we calculate the electric field strength and the displacement amplitude of each GWP and SP branch that correspond to a single quantum of these excitations. This is done by considering the total energy-density expression for SP and GWP and then by setting it equal to $\hbar\omega$. Next these field amplitudes are substituted into the expression for Raman scattering intensities that takes into account the finite scattering volume determined by the film geometry. The Raman-intensity expression for the film geometry was derived by Mills, Chen, and Burstein,[14] and independently by Nkoma and Loudon.[15,16]

The total energy density of SP and GWP is given by[17]

$$W=\sum_\lambda\left[\tfrac{1}{2}(\dot{U}_\lambda^2+\omega_{\mathrm{TO}_\lambda}^2U_\lambda^2)+\frac{1}{8\pi}(\epsilon_{\infty\lambda}E_\lambda^2+H_\lambda^2)\right], \tag{17}$$

where U_λ is the λ Cartesian component of the atomic displacement vector $\vec{U}$, and $\omega_{\mathrm{TO}_\lambda}$ is the TO-phonon frequency with the polarization in the λ direction. The terms in the first set of small parentheses represent the lattice distortion energy and the terms in the second set represent the electromagnetic portion of the energy carried by the polariton. U_λ and H_λ can be expressed in terms of E_λ by

$$U_\lambda=\frac{\omega_{\mathrm{TO}_\lambda}[(\epsilon_{0\lambda}-\epsilon_{\infty\lambda})/4\pi]^{1/2}}{\omega_{\mathrm{TO}_\lambda}^2-\omega^2}E_\lambda \tag{18}$$

and

$$H_\lambda=\frac{ic}{\omega}(\vec{\nabla}\times\vec{E})_\lambda\,. \tag{19}$$

Using Eq. (17) and Eq. (18), we can write the total energy due to SP and GWP contained in a column normal to the film with a unit cross-section area as

$$\overline{W}=2\sum_\lambda\left[S_\lambda(\omega)\int_0^a\langle E_\lambda^2\rangle dz+\frac{1}{8\pi}\int_0^a(\epsilon_{\infty\lambda}\langle E_\lambda^2\rangle+\langle H_\lambda^2\rangle)dz+\frac{1}{8\pi}\int_a^\infty(\langle E_\lambda^2\rangle+\langle H_\lambda^2\rangle)dz\right], \tag{20}$$

where

$$S_\lambda(\omega)=\frac{\omega_{\mathrm{TO}_\lambda}^2(\omega_{\mathrm{TO}_\lambda}^2+\omega^2)(\epsilon_{0\lambda}-\epsilon_{\infty\lambda})}{8\pi(\omega_{\mathrm{TO}_\lambda}^2-\omega^2)^2}\,, \tag{21}$$

and angular brackets enclosing each quantity denote a time average over the period.

With the use of the dispersion relation for each branch of SP and GWP, the coefficients A_λ, B_λ, and C_λ in Eqs. (2), (3), and (4) are determined completely in terms of one free amplitude coefficient. This last degree of freedom corresponds to the degree of excitation, and it is determined by setting[18] $\overline{W}=\hbar\omega$ in Eq. (20). Thus we can fix all the amplitude coefficients A_λ, B_λ, and C_λ which correspond to one quantum of the excitation. Now from Eqs. (2), (3), and (4) we have the expressions for $\langle E_\lambda^2\rangle$ that correspond to the excitation of one quantum of SP or

GWP. (See the Appendix.)

The Raman scattering intensity $I(\Omega)$ per unit film volume can be calculated from the following expression which was adapted from the result of Mills, Chen, and Burstein[14]:

$$I_{\beta\gamma}(\Omega)=\frac{A[n(\Omega)+1]}{2a}\times\left|\sum_{\lambda}\tilde{b}_{\beta\gamma\lambda}(\Omega)\int_{-a}^{a}e^{i\Delta Q_{\perp}z}\langle E_{\lambda}^{2}(z)\rangle^{1/2}dz\right|^{2}\times\delta(\Delta\vec{\mathrm{Q}}_{\parallel}-\vec{\mathrm{k}}_{\parallel})\,, \tag{22}$$

where A is a constant, $\Delta\vec{\mathrm{Q}}=\vec{\mathrm{Q}}_i-\vec{\mathrm{Q}}_s$ is the difference between the wave vector of the incident light $\vec{\mathrm{Q}}_i$ and that of the scattered light $\vec{\mathrm{Q}}_s$; $\langle E_{\lambda}^{2}(z)\rangle^{1/2}$ is the root mean square of the electric field of the polariton discussed above, $n(\Omega)$ is the Bose-Einstein factor, and $\Omega=\omega_i-\omega_s$ is the difference between the incident-light frequency ω_i and the scattered-light frequency ω_s. $\tilde{b}_{\beta\gamma\lambda}(\Omega)$ is given by

$$\tilde{b}_{\beta\gamma\lambda}(\Omega)=b_{\beta\gamma\lambda}+\left[\frac{\epsilon_{\lambda}(\Omega)-\epsilon_{\infty\lambda}}{4\pi Ne_{\lambda}^{*}}\right]a_{\beta\gamma\lambda}\,, \tag{23}$$

where N is the number of unit cells per unit volume, e_{λ}^{*} is the transverse effective charge of the λ-polarized pure TO phonon, $b_{\beta\gamma\lambda}$ is the electro-optic coefficient, and $a_{\beta\gamma\lambda}$ is the atomic displacement susceptibility tensor[18]; β and γ denote the polarization of the scattered and the incident light, respectively. Ne_{λ}^{*} in Eq. (25) can be determined from the oscillator strength of the TO phonon with λ polarization, and the ratio $b_{\beta\gamma\lambda}/a_{\beta\gamma\lambda}$ can be determined from the ratio of the TO-phonon and the LO-phonon scattering intensities, $I(\omega_{\mathrm{LO}_{\lambda}})/I(\omega_{\mathrm{TO}_{\lambda}})$.[19] Thus $\tilde{b}_{\beta\gamma\lambda}(\Omega)$ can be determined experimentally within a multiplicative constant. By using $\langle E_{\lambda}^{2}(z)\rangle^{1/2}$ from the polariton-energy-density expressions, we can write down the complete expression for the Raman scattering intensity given by Eq. (22) with one multiplicative constant still undetermined but common for all thicknesses and branches. As we see in the Appendix, the Raman scattering intensity for GWP contains expressions such as

$$\left[\frac{\sin[(\Delta Q_{\perp}-k_{\perp})a]}{\Delta Q_{\perp}-k_{\perp}}\pm\frac{\sin[(\Delta Q_{\perp}+k_{\perp})a]}{\Delta Q_{\perp}+\vec{\mathrm{k}}_{\perp}}\right]^{2}. \tag{24}$$

This factor represents the uncertainy in k_z due to the finite interaction length in the film confined within $-a\leq z\leq a$ along the surface normal. (In the present experiment $\alpha d\leq 1$; so the effect of sample thickness dominates over the effect of absorption in determining the uncertainty in $k_{\perp}$.) For SP the corresponding factor has the form $(\beta^2+\Delta Q_{\perp}^2)^{-1}$ in the limit of $d\rightarrow\infty$.

Figure 7 illustrates the calculated Raman spectra of SP and GWP for ϵ-GaSe of thicknesses 2.7 and 6.5 μm. The film surface is assumed to be normal to the c axis, and the exciting laser beam at 5145 Å is incident on the film normal to the surface. The $k_{\parallel}$ values of 10^4 and 3500 cm^{-1} correspond to near-forward scattering angles. For each line the mode-damping constant of 0.5 cm^{-1} is assumed. The ratio of $I(\omega_{\mathrm{LO}_{\perp}})/I(\omega_{\mathrm{TO}_{\perp}})$ is set equal to the measured value of 3.5. We note that two or three peaks appear for each group of GWP branches. This is a result of the relaxation of the wave-vector conservation along the thickness of the film. Also note that in the thicker film (6.5 μm) the SP peak is weak relative to the GWP peaks while they have comparable intensities in the thinner film (2.7 μm). This is due to the fact that the field strength of SP is localized at the surface. In contrast, most of the field strength of GWP is spread inside the film; hence the GWP intensity increases with film thickness.

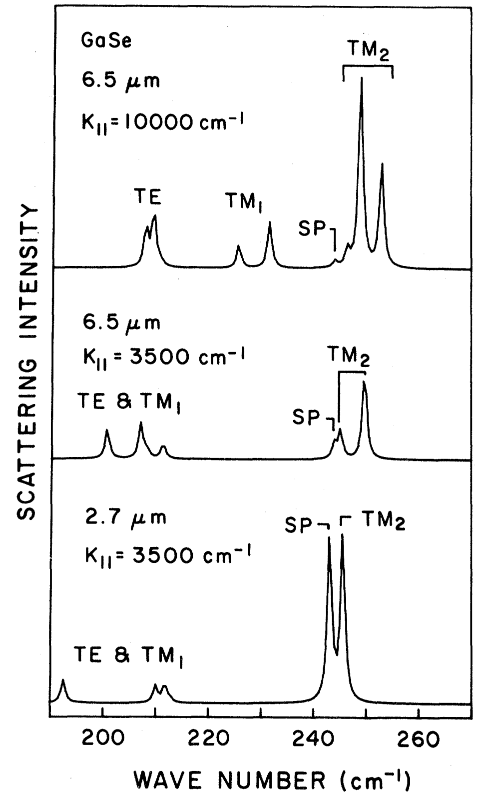

FIG. 7. Raman spectra of GWP and SP for ϵ-GaSE calculated from Eq. (22).

III. EXPERIMENT

Single crystals of ϵ-GaSe were grown by the Bridgman method and the polytype was determined to be of the ϵ-type using x-ray diffraction and Raman scattering. The thin-film samples used in the present experiment were prepared by cleaving a large bulk sample. The thickness of the film was determined from the period of a Fabry-Perot—type transmission spectrum obtained by a beam of white light normally incident on the film. In calculating the thickness we used the value of the refractive index derived from ellipsometry measurements.[20] The uncertainty in the measured film thickness is estimated to be less than ±10%.

Raman scattering measurements were made at room temperature using the 5145-Å line of an argon-ion laser as the excitation source. The incident beam of 50 mW (cw) was directed normal to the film surface, and the spectrum of the scattered light emerging in the near-forward direction at varied angles was measured. In order to collect all the light emerging at a given scattering angle, we used an annular aperture, and aligned the directly transmitted beam to fall at the center of the blocked portion of the annular aperture. The experimental geometry was identical to the one shown in Ref. 2. At 5145 Å the absorption coefficient of ϵ-GaSe is 2×10^3 cm^{-1}, which corresponds to the skin depth of 5 μm. The range of sample thickness was 2.7 to 6.5 μm. Thus a sufficient amount of the scattered light could emerge in the forward direction even after absorption within the sample. The incident laser energy is more than 0.4 eV away from the nearest band edge; hence, we did not have to be concerned about the variation of the resonance enhancement factor within the measured frequency range.

The Raman-intensity data were collected digitally using a Digital Equipment Corporation LSI-11 minicomputer interfaced to a double grating spectrometer and photon counting electronics via a CAMAC system. Typical photon counting rates for the GWP peaks were in the range of 1 to 100 counts per sec with the spectral resolution set at 3 cm^{-1} and the scattering angle resolution set between 10% (for $k_{\parallel}\geq5000$ cm^{-1}) and 30% ($k_{\parallel}\leq4000$ cm^{-1}). The accumulation time necessary to obtain a reasonable signal-to-noise ratio was 60 to 120 sec for each spectral data point. The incident laser beam was linearly polarized, and the scattered light was collected for all polarizations.

In order to compare the calculated Raman intensities with the measured values, it is necessary to normalize the measured spectrum against a standard that does not vary with the scattering angle θ_p (or $k_{\parallel}$) or from one run to another due to changes in minor optical alignment. We used the A'_1 mode that appears at 135 cm^{-1} as the intensity calibration standard. Since the A'_1 mode is nonpolar, its scattering intensity does not depend on the scattering angle, and it is proportional to the film thickness. The A'_1-mode intensity does depend on the polarization of the incident and the scattering light; however, since the light polarization is kept essentially normal to the c axis in all of the measurements, the polarization dependence does not affect our results. Thus by taking the relative intensities of the GWP and SP peaks with respect to the A'_1-mode intensity in each spectrum, we automatically make corrections for the variation in the solid angle of collection, sample thickness, scattering angle, and other parameters that vary from run to run. The accuracy of this normalization procedure is estimated to be about ±10%.

The Raman spectra of volume polaritons propagating with a large wave vector ($k\simeq10^5$ cm^{-1}) were obtained first (Fig. 2). As we indicated in Sec. I, these spectra agree with the expected selection rules; furthermore, the peak positions give the frequencies of the TO$_{\perp}$ and LO$_{\perp}$ phonons listed in Table I. Figure 8 shows an example of the Raman spectra of GWP's measured at $k_{\parallel}=13\,500$ cm^{-1} for two samples of thickness, 2.7 and 6.5 μm. The peak at $\sim$210 cm^{-1} is due to TE GWP and the prominent peak at $\sim$250 cm^{-1} is due to TM$_2$ GWP. The frequencey of these modes does not depend sensitively on the sample thickness. The very weak peak between the two large peaks is due to TM$_1$ GWP. The frequency of this mode is a sensitive function of the film thickness. We note that the scattering intensity per unit volume is higher in the 6.5-μm sample than in the 2.7-μm sample by a factor of 1.3. The (upper) TE$_u$ and (upper) TM$_u$ modes lie far above the frequency range shown in Fig. 8. We did not attempt to observe these modes in this paper.

The dispersion of the observed GWP's and SP (squares) are compared with the theoretical predictions (solid curves) in Figs. 9 and 10 for the two samples of thickness, 2.7 and 6.5 μm. The theoretical dispersion curves are shown only for branches for which the relaxed wave-vector conservation rule, $|\Delta Q_{\perp}-k_{\perp}|a<\pi$, is satisfied. The branches that do not satisfy this selection rule are expected to contribute very weak Raman spectrum as we have indicated in Sec. II B. In both Figs. 9 and 10 we see that only the strongest branches are detected in our spectra, and that many weaker branches allowed by the above $k_{\perp}$-selection rule do not appear in the observed spectra.

Figures 11 and 12 show the theoretical fit of the Raman spectra of GWP and SP for different values of $k_{\parallel}$ (equivalent to different scattering angles) and

TABLE I. Dielectric constants and polar phonon frequencies (cm^{-1}) of ϵ-GaSe.

	ir[a]	ir[b]	ir[c]	ir[d]	Raman[e]	Capacitance[f]	Present work
$\epsilon_{0\perp}$	10.6	10.6	9.8				9.8
$\epsilon_{0\parallel}$		6.18		6.22		8.0±0.3	7.6
$\omega_{\mathrm{TO}_\perp}$	211	213.5	211.6		215±2		213.0
$\omega_{\mathrm{LO}_\perp}$		254.7	253.8		252.1		254.2
$\omega_{\mathrm{TO}_\parallel}$		237.0		236.5			236.0
$\omega_{\mathrm{LO}_\parallel}$		245.5		246.0			244.5

[a] Reference 21.
[b] Reference 10.
[c] Reference 22.
[d] Reference 23.
[e] Reference 8.
[f] Reference 9.

for the two sample thicknesses. The theoretical spectra were generated using Eq. (22) with the following procedure. First, $\omega_{\mathrm{TO}_\perp}$ and $\omega_{\mathrm{LO}_\perp}$ were determined from the spectra of Fig. 2. Since the dispersion of TE GWP is determined completely by $\omega_{\mathrm{TO}_\perp}$, $\omega_{\mathrm{LO}_\perp}$, and $\epsilon_{0\perp}$, the value of $\epsilon_{0\perp}$ was fixed by fitting the theoretical dispersion curve of TE GWP to the data points. Second, $\epsilon_{\infty\perp}$ was calculated from the Lyddane-Sacks-Teller relation using the values for $\omega_{\mathrm{TO}_\perp}$, $\omega_{\mathrm{LO}_\perp}$, and $\epsilon_{0\perp}$. The remaining parameters $\omega_{\mathrm{TO}_\parallel}$, $\omega_{\mathrm{LO}_\parallel}$, and $\epsilon_{0\parallel}$ were determined by fitting the dispersion curves for TM_1-GWP and TM_2-GWP branches. The values of these parameters that produce the best fit to the observed dispersion relations of the three branches are summarized in Table I. The uncertainties for the values of ϵ's and the listed frequencies are ±0.3 and ±0.75 cm^{-1}, respectively. The present results for the phonon frequencies, $\epsilon_{0\perp}$, and $\epsilon_{\infty\perp}$ show good agreement with the previously obtained values from the ir measurements[10,21–23] and the Raman measurements at large wave vectors[8] ($k \simeq 10^5$ cm^{-1}). However, the present values of $\epsilon_{0\parallel}$ and $\epsilon_{\infty\parallel}$ show a significant deviation from the ir measurement results.[10,23]

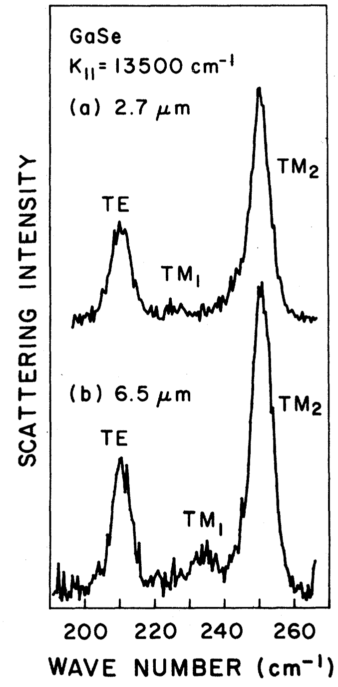

FIG. 8. Raman spectra of thin films of ϵ-GaSe for (a) $d = 2.7$ μm and (b) $d = 6.5$ μm at $k_\parallel = 13\,500$ cm^{-1}.

When the above-mentioned parameters are fixed, Eq. (22) contains only two free parameters. One of them is the constant A which determines the abso-

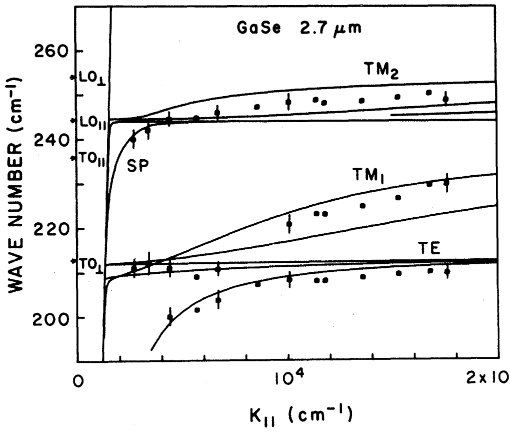

FIG. 9. Measured (squares) and calculated (solid lines) dispersion curves of GWP and SP for the 2.7-μm film. The calculated dispersion curves include only the branches satisfying $|\Delta Q_\perp - k_\perp| a < \pi$.

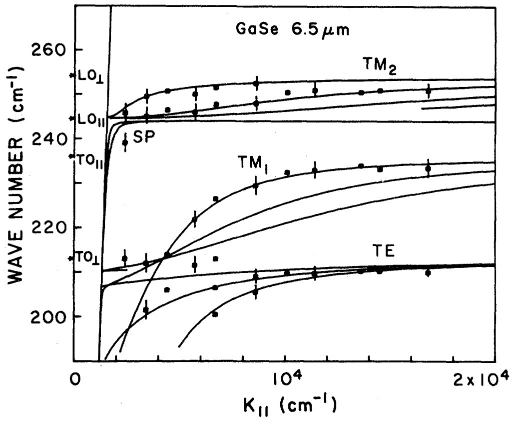

FIG. 10. Measured (squares) and calculated (solid lines) dispersion curves of GWP and SP for the 6.5-μm film.

lute scattering intensity. Since we can measure only relative Raman intensities, we leave this constant adjustable. The other parameter still undetermined is the ratio $b_{\beta\gamma\lambda}/a_{\beta\gamma\lambda}$. This ratio is determined from the intensity ratio of the TO$_\perp$- and LO$_\perp$-phonon peaks shown in Fig. 2.[24] When we follow this procedure, we can generate the theoretical Raman scattering intensity curves for all values of $k_\|$ and sample thicknesses with only one overall adjustable parameter $Aa_{\beta\gamma\lambda}^2$ of Eq. (22). The theoretical spectra that are compared with the data points in Figs. 11 and 12 were generated in this manner; i.e., all the curves in Figs. 11 and 12 were calculated using a single set of parameters changing only the value of $k_\|$ and the sample thickness d. The line shape of each peak was assumed to be Lorentzian with the full width at half maximum (FWHM) of 5.0 cm^{-1}. This value of the linewidth was deduced from the spectra in Fig. 2. Thus we are assuming the mode damping to be independent of frequency and sample thickness. As we can see in Figs. 11 and 12, the theoretical spectra agree quite well with the measured Raman spectra with a few exceptions. This degree of agreement is particularly remarkable considering the fact that a single set of common parameters are used without any adjustable parameter for all the dozen spectra shown in Figs. 11 and 12.

IV. DISCUSSION

In this section we will first discuss the differences between the observed Raman intensities and the theoretical predictions. We find that the agreement between theory and experiment is better for thicker samples than for thinner samples. This observation leads us to consider the effect of surface roughness on phonon damping, and we will discuss damping of phonons upon reflection from the crystal surface. Finally, we will discuss the values of dielectric parameters obtained from the present experiment and make some comparisons with earlier results.

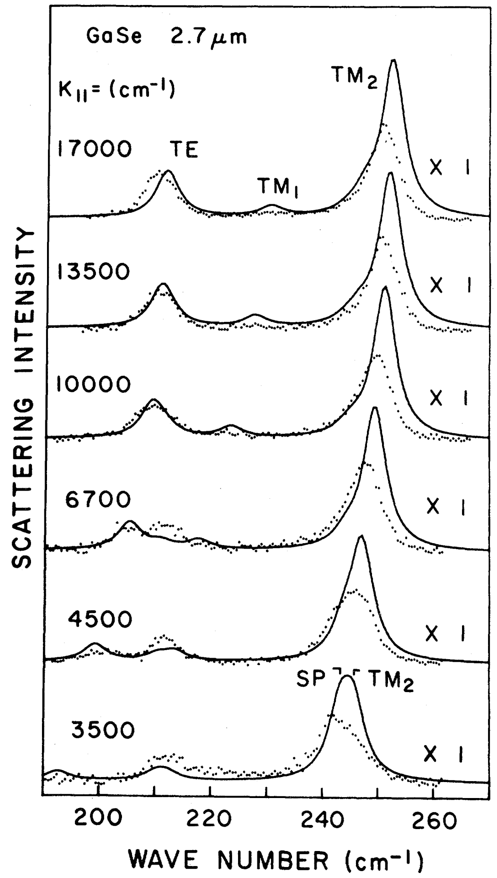

FIG. 11. Measured (dots) and calculated (solid lines) Raman spectra of GWP and SP of the 2.7-μm sample. The vertical scale is common for all the spectra here and in Fig. 12.

A. Raman scattering intensity

In a crystal with D_{3h}^1 symmetry the Raman tensor elements $b_{\beta\gamma z}$ ($\beta,\gamma = x,y,z$) are zero for the E' modes. Hence, there is no contribution to the Raman scattering intensity from the z component of the $\vec{E}$ field (E_z). This selection rule causes rapid decrease of the Raman intensity as the GWP frequencies approach $\omega_{\mathrm{TO}_\|}$ or $\omega_{\mathrm{LO}_\|}$, because near $\omega_{\mathrm{TO}_\|}$ (or $\omega_{\mathrm{LO}_\|}$) GWP's consist mostly of the z-polarized TO$_\|$ (or LO$_\|$) phonon. The effect of this selection rule could be clearly seen in many of the calculated spectra (not shown here), although it is not very clearly shown in Figs. 11 or 12 due to the broadness of the lines. Agreement with this selection rule was used as a

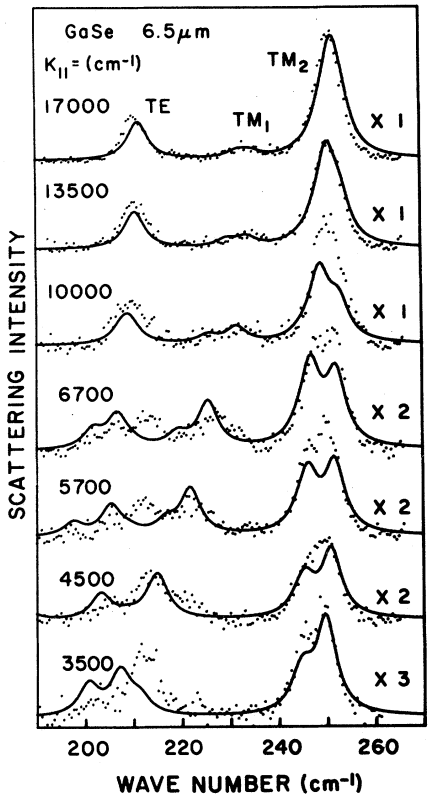

FIG. 12. Measured (dots) and calculated (solid lines) Raman spectra of GWP and SP for 6.5-μm sample.

check of the basic soundness of the calculated spectra.

The Raman tensor $\tilde{b}_{\beta\gamma\lambda}$ goes through a zero at 158 cm^{-1} due to the cancellation between the $a_{\beta\gamma\lambda}$ and $b_{\beta\gamma\lambda}$ terms in Eq. (23). Experimentally, the Raman intensity decreases toward lower frequencies below $\omega_{\mathrm{TO}_\perp}$, and no GWP peak was observed below 190 cm^{-1}. In contrast to the suggestion given in the previous work on GWP of GaP,[5] the generally good agreement seen in Figs. 11 and 12 indicates that the theory based on the bulk Raman tensor is appropriate for GWP's in thin films down to a few micrometers. This conclusion is reasonable, since GWP is essentially a volume polariton in a confined geometry. It is also consistent with the experimental results for SP in GaP,[25] where the Raman selection rule was found to be determined by the bulk Raman tensor. We must conclude that the anomalous results found by VMU[5] was caused by extrinsic conditions such as surface roughness.

As we have described earlier, the necessary parameters for spectral calculations were fixed using the top spectrum of Fig. 12 for the 6.5-μm sample at $k_{\parallel}=17\,000\ \mathrm{cm}^{-1}$. Thus naturally the fit is best for that spectrum. The cause for the excess of the observed intensity for $4500\ \mathrm{cm}^{-1} \leq k_{\parallel} \leq 10\,000\ \mathrm{cm}^{-1}$ around the TM_2 peak in the 6.5-μm sample (Fig. 12) is not known at this time. An extra peak seen in these spectra at 213 cm^{-1} is due to the reflection of the backscattering by TE and TM_1 GWP's with large $k_\perp$ values ($k_\perp \simeq 2\times10^5\ \mathrm{cm}^{-1}$). In our simplified formulation of Raman intensities, backscattering processes were not included; hence, the theoretical curves do not show a peak here. The backscattering by TM_2 GWP with large $k_\perp$ values does not appear in the spectra, because it is polarized mostly along the z direction and $\tilde{b}_{\beta\gamma z}$ is zero.

The dispersion curves in Figs. 9 and 10 were drawn with the assumption that the peaks for which the wave-vector conservation condition $|\Delta Q_\perp - k_\perp|\, a < \pi$ is satisfied will appear in the spectra. However, we see in Figs. 9 and 10 that some of the branches that satisfy this condition are not observed experimentally. This difference arises because all peaks are broad and some weak peaks are masked by a neighboring stronger peak. In fact, some of the peaks cannot be resolved in the calculated spectra of Figs. 11 and 12. For example, three TM_2-GWP and SP peaks are well resolved for $d=6.5\ \mu\mathrm{m}$ and $k_{\parallel}=10\,000\ \mathrm{cm}^{-1}$ when the damping widths are assumed to be narrow (Fig. 7), but these four peaks merge into one peak and a shoulder in the third spectrum of Fig. 12, where the actual damping width is greater. We note in Fig. 9 that, for the 2.7-μm sample, the observed peak positions are consistently lower than the expected value. This observation is discussed below.

Although the agreement between the calculated and the experimental spectra is remarkable, we note that the discrepancy between the two spectra is greater for the 2.7-μm sample than for the 6.5-μm sample. The agreement for a 5.4-μm sample (spectra not shown) is similar to the 6.5-μm sample. The peak positions in the 2.7-μm sample are approximately 3 cm^{-1} lower than expected and the peak intensities are noticeably lower than the calculated result particularly for TM_2 GWP (see Fig. 11). We can obtain a better fit between theory and experiment if we assume that the mode-damping parameter is greater for the 2.7-μm sample than for the 6.5-μm sample. This dependence of the damping parameter on sample thickness can be understood, if the mean free path of the bulk mode is much longer than the sample thickness and significant damping occurs as GWP is reflected at the surface. This line of reasoning is detailed in what follows.

B. Damping of GWP at the surface

In the zigzag propagation picture of GWP shown in Fig. 6, GWP is totally reflected at the film surface. Imperfections at the surface, such as roughness or a dust particle, cause diffuse scattering of GWP. Tiny steps introduced in the cleaving process are probably the origin of surface imperfections in our GaSe samples. In this imperfect reflection process some part of GWP is radiated into air or converted into other GWP and/or SP. These loss mechanisms contribute to increased damping. In the following discussion we assume that these loss mechanisms are unimportant for the nonpolar A'_1 mode that we use for intensity calibration.

The GWP intensity after n_r reflections at the crystal surface is

$$I(n_r)=I(0)R^{n_r} , \tag{25}$$

where R is the intensity reflection coefficient very close to unity. The effective mean free path L of GWP is then given by

$$\frac{1}{L}=\frac{1}{l_b}+\frac{\cos\theta_p}{Nd} , \tag{26}$$

where l_b is the mean free path of the bulk polariton, and $N=-1/\ln R$ is the number of reflections after which the GWP intensity decreases to $1/e$ of the original value. We assume here $R=0.99$, and then $N=99$. l_b can be written in terms of the bulk polariton damping constant Γ as

$$l_b=\frac{\omega}{\Gamma}\frac{2\pi}{k} . \tag{27}$$

For $\Gamma=2$ cm^{-1} and $k=2\times10^4$ cm^{-1}, $l_b\simeq400$ μm. In comparison $Nd/\cos\theta_p$ in Eq. (26) is much longer in the 6.5-μm sample; hence, the effect of reflection loss is not very important in the 6.5-μm sample. On the other hand, $Nd/\cos\theta_p$ becomes comparable or less than l_b in the 2.7-μm sample. Since we have chosen the spectral parameters by optimizing the fit for the 6.5-μm sample, the damping caused by surface reflection ($Nd/\cos\theta_p$ term) did not affect the relative intensity for different $k_{||}$. In the 2.7-μm sample the surface reflection damping plays an important role in reducing L of Eq. (26). Thus the fit for this sample is worse than for the 6.5-μm sample. At some k values, L may become as short as 200 μm in the 2.7-μm sample. Since the peak Raman intensity scales with L, we may make an error of as much as 50% for the peak intensities in the 2.7-μm sample. We believe that this shortening of the mean free path in the thinner sample is the main cause of discrepancies seen in Fig. 11. Since frequency shift and damping correspond to the real and imaginary parts of the surface-induced variation in self-energy, it is not surprising that a shift of peak positions on the order of ~3 cm^{-1} is also observed in the 2.7-μm sample. Similar effects were observed on a roughened GaP surface.[26]

In the case of polished samples that were used by VMU, the crystal surfaces are expected to be much rougher than that of the samples used in this work. In estimating the values of L for GaSe, we assumed the reflectivity R to be 0.99. But at a polished surface of GaP, R should be appreciably lower. If we assume $R=0.9$, the number of reflections within one mean free path will be only nine times. Then there will be an uncertainty in $k_{||}$ as well as in $k_\perp$. The uncertainty in $k_{||}$ will broaden the linewidths, and the uncertainty in $k_\perp$ will relax the $k_\perp$ conservation even more than is indicated by Eq. (24). The net consequence will be to increase the number of GWP peaks that can be observed by Raman scattering. This may be the situation that VMU observed in the GaP slabs.

This appears to be the first time that the effect of a finite sample size was clearly observed on polariton damping. The sample-size effect on polariton damping is an interesting subject that deserves more detailed theoretical and experimental investigation. Further details on this effect will be reported in a separate paper when more experimental evidence is accumulated.

C. Dielectric constants

The parameters used in the calculation of the dispersion relations of GWP's and SP's are summarized in Table I. Although the dielectric constant for $\perp$ polarization and the polar phonon frequencies derived in this paper agree well with those reported earlier, the dielectric constant for $||$ polarization shows considerable discrepancy between the present result and the value derived from the ir reflection spectrum.[10,23] The ir measurements to deduce the parameters for $||$ polarization were performed on polished surfaces normal to the layer. Such surfaces are not smooth but are damaged in the polishing process. The effective dielectric constant $\epsilon_{0||}$ at damaged surfaces is likely to be different from the bulk value. Indeed, our $\epsilon_{0||}$ agrees with the value derived from capacitance measurements for cleaved films.[9] Ushioda *et al.*[26] suggested that the dielectric constant decreases near a GaP surface which is roughened by polishing. $\epsilon_{0||}$ derived for a polished surface in ϵ-GaSe is also smaller than $\epsilon_{0||}$ deduced in this work or by capacitance measurements.

V. CONCLUSION

The Raman spectra of GWP and SP in thin films with atomically smooth surfaces were measured in cleaved ϵ-GaSe films with the thickness of several micrometers. Although the dispersion of GWP in ϵ-GaSe is quite complicated, the measured scattering intensities and the dispersion relations of GWP and

SP agree very well with theoretical calculations based on the bulk Raman tensor. In the thinnest 2.7-μm sample, however, the measured scattering intensity is appreciably weaker than the theoretical expectation. Using the picture of zigzag propagation of GWP, this discrepancy can be explained in terms of the scattering of GWP by surface imperfections upon reflection. In polished samples, which may contain much more surface imperfections than cleaved surfaces, scattering of GWP by surface imperfections is expected to modify the Raman spectra and dispersion relations considerably.

Note added in proof. Very recently we found that the main cause of disagreement between theory and experiment for the spectrum of the 2.7-μm sample (Fig. 11) was due to heating of the sample by the exciting laser beam. When we changed the incident laser wavelength to 6328 Å, where absorption is essentially negligible ($\alpha d \simeq 0$), both the peak positions and the intensities of GWP agree well with those of the calculated spectrum. By taking into account the backscattering contribution from $\mathrm{TO}_{\perp}$ and the uncertainties in θ_s, we obtained theoretical spectra that agree well with the measured results for both samples; this could be accomplished without invoking the effect of surface roughness.

ACKNOWLEDGMENT

This work was supported in part by the U.S. Air Force Office of Scientific Research Grants No. 77-3222 and No. 82-0086.

APPENDIX

Here we exhibit the explicit expressions that were used in calculating the Raman spectra of SP and GWP. For clarity we write down the six dispersion relations presented in Sec. II and assign the branch designations:

For TM(t) GWP

$$\epsilon_{\perp}/\epsilon_1 = (k_{\perp}/\alpha)\tan(k_{\perp}a) \; . \qquad \text{(A1)}$$

For TM(c) GWP

$$\epsilon_{\perp}/\epsilon_1 = -(k_{\perp}/\alpha)\cot(k_{\perp}a) \; . \qquad \text{(A2)}$$

For TE(t) GWP

$$1 = (k_{\perp}/\alpha)\tan(k_{\perp}a) \; . \qquad \text{(A3)}$$

For TE(c) GWP

$$1 = -(k_{\perp}/\alpha)\cot(k_{\perp}a) \; . \qquad \text{(A4)}$$

For UM-SP

$$\epsilon_{\perp}/\epsilon_1 = -(\beta/\alpha)\tanh(\beta a) \; . \qquad \text{(A5)}$$

For LM-SP

$$\epsilon_{\perp}/\epsilon_1 = -(\beta/\alpha)\coth(\beta a) \; . \qquad \text{(A6)}$$

When these dispersion relations are used in conjunction with the relations derived from the Maxwell equations and the boundary conditions A_{λ}, B_{λ}, and C_{λ} of Eqs. (2)–(4) can be expressed in terms of one of B_{λ}'s for each branch. Then the resultant expressions for E_{λ} and H_{λ} are substituted in Eq. (20). When we set $\overline{W} = \hbar\omega$, we can solve the equation for the undetermined coefficient B_x, B_y, or B_z. The following shows the expressions for B_{λ}^2 for each branch.

For TM(t) GWP

$$B_x^2 = \hbar\omega \left[\frac{S_{\perp}p^{-} + S_{\parallel}f^2p^{+}}{k_z} + \frac{1}{8\pi}\left[\frac{2k_x^2\sin^2\theta}{\alpha^3} + \frac{\epsilon_{\infty\perp}p^{-} + \epsilon_{\infty\parallel}f^2p^{+} + (c/\omega)^2(k_z+fk_x)^2p^{+}}{k_z} \right] \right]^{-1} . \qquad \text{(A7)}$$

For TM(c) GWP

$$B_x^2 = \hbar\omega \left[\frac{S_{\perp}p^{+} + S_{\parallel}f^2p^{-}}{k_z} + \frac{1}{8\pi}\left[\frac{2k_x^2\cos^2\theta}{\alpha^3} + \frac{\epsilon_{\infty\perp}p^{+} + \epsilon_{\infty\parallel}f^2p^{-} + (c/\omega)^2(k_z+fk_x)^2p^{-}}{k_z} \right] \right]^{-1} . \qquad \text{(A8)}$$

For TE(t) GWP

$$B_y^2 = \hbar\omega \left[\frac{S_{\perp}p^{+}}{k_z} + \frac{1}{8\pi}\left[\frac{(1+c^2(\alpha^2+k_x^2)/\omega^2)\cos^2\theta}{\alpha} + \frac{\epsilon_{\infty\perp}p^{+} + (c/\omega)^2(p^{-}k_z^2 + p^{+}k_x^2)}{k_z} \right] \right]^{-1} . \qquad \text{(A9)}$$

For TE(c) GWP

$$B_y^2 = \hbar\omega \left[\frac{S_{\perp}p^{-}}{k_z} + \frac{1}{8\pi}\left[\frac{(1+c^2(\alpha^2+k_x^2)/\omega^2)\sin^2\theta}{\alpha} + \frac{\epsilon_{\infty\perp}p^{-} + (c/\omega)^2(p^{+}k_z^2 + p^{-}k_x^2)}{k_z} \right] \right]^{-1} . \qquad \text{(A10)}$$

For UM SP

$$B_x^2=\hbar\omega\left[\frac{S_\perp q^- + S_{||} f^2 q^+}{\beta}+\frac{1}{8\pi}\left[\frac{2k_x^2\sinh^2\theta}{\alpha^3}+\frac{\epsilon_{\infty\perp} q^- + \epsilon_{\infty ||} f^2 q^+ + (c/\omega)^2(\beta-k_x f)^2 q^+}{\beta}\right]\right]^{-1} . \tag{A11}$$

For LM SP

$$B_x^2=\hbar\omega\left[\frac{S_\perp q^+ + S_{||} f^2 q^-}{\beta}+\frac{1}{8\pi}\left[\frac{2k_x^2\cosh^2\theta}{\alpha^3}+\frac{\epsilon_{\infty\perp} q^+ + \epsilon_{\infty ||} f^2 q^- + (c/\omega)^2(\beta-k_x f)^2 q^-}{\beta}\right]\right]^{-1} . \tag{A12}$$

Here

$$\theta=\begin{cases} k_z a & \text{for GWP} \\ \beta a & \text{for SP ,} \end{cases} \tag{A13}$$

$$f=\begin{cases} k_x\epsilon_\perp(\omega)/[k_z\epsilon_{||}(\omega)] & \text{for GWP} \\ k_x\epsilon_\perp(\omega)/[\beta\epsilon_{||}(\omega)] & \text{for SP ,} \end{cases} \tag{A14}$$

$$p^\pm=\theta\pm\tfrac{1}{2}\sin(2\theta) , \tag{A15}$$

$$q^\pm=\pm\theta+\tfrac{1}{2}\sinh(2\theta) , \tag{A16}$$

and $S_\perp = S_{x,y}(\omega)$ and $S_{||}=S_z(\omega)$ are defined in Eq. (21).

Finally the expression

$$\left|\int_{-a}^{a} e^{i\Delta Q_\perp z}\langle E_\lambda^2(z)\rangle^{1/2}dz\right|^2$$

in Eq. (22) is given in terms of B_λ^2 by

$$\left[\frac{\sin[(\Delta Q_\perp - k_z)a]}{\Delta Q_\perp - k_z}\pm\frac{\sin[(\Delta Q_\perp + k_z)a]}{\Delta Q_\perp + k_z}\right]^2 B_\lambda^2 \quad \text{(for GWP)} , \tag{A17}$$

where the + sign is for modes with the electric field of the form

$$\langle E_\lambda^2(z)\rangle^{1/2}=B_\lambda\cos(k_z z) , \tag{A18}$$

and the − sign is for modes with the electric field of the form

$$\langle E_\lambda^2(z)\rangle^{1/2}=B_\lambda\sin(k_z z) , \tag{A19}$$

and the same expression is given as

$$4\left[\frac{\beta\sin(\Delta Q_\perp a)\cosh(\beta a)-\Delta Q_\perp\cos(\Delta Q_\perp a)\sinh(\beta a)}{\beta^2+\Delta Q_\perp^2}\right]^2 B_\lambda^2 \quad \text{(for SP)} , \tag{A20}$$

when

$$\langle E_\lambda^2(z)\rangle^{1/2}=B_\lambda\sinh(\beta z) , \tag{A21}$$

and as

$$4\left[\frac{\beta\cos(\Delta Q_\perp a)\sinh(\beta a)+\Delta Q_\perp\sin(\Delta Q_\perp a)\cosh(\beta a)}{\beta^2+\Delta Q_\perp^2}\right]^2 B_\lambda^2 \quad \text{(for SP)} , \tag{A22}$$

when

$$\langle E_\lambda^2(z)\rangle^{1/2}=B_\lambda\cosh(\beta z) . \tag{A23}$$

[*] Permanent address: The Research Institute for Iron, Steel and Other Metals, Tohoku University, Sendai 980, Japan.

[1] A. Otto, in *Festkörperprobleme,* Advances in Solid State Physics, edited by J. Freusch (Vieweg, Braunschweig, 1974), Vol. XIV, p. 1.

[2] S. Ushioda, in *Progress in Optics,* edited by E. Wolf (North-Holland, Amsterdam, 1981), Vol. XIX, Chap. III.

[3] K. L. Kliewer and R. Fushs, Phys. Rev. 144, 495 (1966).

[4] P. K. Tien, Rev. Mod. Phys. 49, 361 (1977).

[5] J. B. Valdez, G. Mattei, and S. Ushioda, Solid State Commun. 27, 1089 (1978).

[6] K. R. Subbaswamy and D. L. Mills, Solid State Commun. 27, 1085 (1978).

[7] H. Yoshida, S. Nakashima, and A. Mitsuishi, Phys. Status Solidi B 59, 655 (1973).

[8] J. C. Irwin, R. M. Hoff, B. P. Clayman, and R. A. Bromley, Solid State Commun. 13, 1531 (1973).

[9] P. C. Leung, G. Anderman, W. G. Spitzer, and C. A. Mead, J. Phys. Chem. Solids 27, 849 (1966).

[10] R. Le Toullec, N. Piccioli, M. Mejatty, and M. Balkanski, Nuovo Cimento 38B, 159 (1977).

[11] R. Loudon, Adv. Phys. 13, 423 (1964).

[12] R. M. Hoff, J. C. Irwin, and R. M. A. Lieth, Can. J. Phys. 53, 1606 (1975).

[13] H. J. Falge and A. Otto, Phys. Status Solidi B 56, 523 (1973).

[14] D. L. Mills, Y. J. Chen, and E. Burstein, Phys. Rev. B 13, 4419 (1976).

[15] J. S. Nkoma and R. Loudon, J. Phys. C 8, 1950 (1975).

[16] J. S. Nkoma, J. Phys. C 8, 3919 (1975).

[17] K. Huang, Proc. R. Soc. London Ser. A 208, 352 (1951).

[18] E. Burstein, S. Ushioda, and A. Pinczuk, Solid State Commun. 6, 407 (1968).

[19] S. Ushioda, A. Pinczuk, W. Taylor, and E. Burstein, in *Proceedings of the International Conference on II-VI Semiconducting Compounds, Brown University, 1967,* edited by D. G. Thomas (Benjamin, New York, 1967), p. 1185.

[20] F. Meyer, E. E. de Kluizenaar, and D. den Engelsen, J. Opt. Soc. Am. 63, 529 (1973).

[21] N. Kuroda, Y. Nishina, and T. Fukuroi, J. Phys. Soc. J. 28, 981 (1970).

[22] K. R. Allakhverdiev, S. S. Babaev, and M. M. Tagiev, Phys. Status Solidi B 93, K67 (1979).

[23] V. Riede, H. Neumann, H. Sobotta, and F. Levy, Solid State Commun. 34, 229 (1980).

[24] Actually, two possible values of $b_{\beta\gamma\lambda}/a_{\beta\gamma\lambda}$ result from the measured value of $I(\mathrm{LO}_\perp)/I(\mathrm{TO}_\perp)$, but one of them gives wrong intensities for polaritons below $\omega_{\mathrm{TO}_\perp}$ (see Ref. 19).

[25] J. B. Valdez and S. Ushioda, Phys. Rev. Lett. 38, 1098 (1977).

[26] S. Ushioda, A. Aziza, J. B. Valdez, and G. Mattei, Phys. Rev. B 19, 4012 (1979).